RSC Advances

ROYAL SOCIETY OF CHEMISTRY

www.rsc.org/advances

α -MoO_3 nanoparticles: Solution combustion synthesis, photocatalytic and electrochemical properties

G. P. Nagabhushana[a], D. Samrat[b] and G. T. Chandrappa[a]*
[a]Department of Chemistry, Bangalore University, Bangalore-560001, India
[b]Center for Nano and Materials Sciences, Jain University, Jakkasandra-562112, India

Abstract

Nanoparticles of ultra-porous MoO_3 have been synthesized in a single step by solution combustion reaction using molybdenum metal powder for the first time as precursor. The effects of the preparation conditions such as the temperature and precursor concentration on the crystalline phase and morphology of the products have been studied systematically. The analytical techniques SEM, TEM, PXRD, TGA, FTIR, and SAED have been used to characterize the morphology, composition, and structure of the as-prepared products. The TEM images of MoO_3 show that the particles are in the range of 2-10 nm. Electrochemical characterization of MoO_3 has been done in 0.5 M H_2SO_4. Specific capacitance and electrochromic property of MoO_3 has been studied. The high photocatalytic activity of MoO_3 has been investigated using Methylene blue azo-dye at various concentrations. It has shown 100 % degradation of high concentration of about 75 mg L^{-1}.

*To whom correspondence should be addressed.
E-mail address: gtchandrappa@yahoo.co.in, Tel.: +91 80 22961350.

1. Introduction

Synthesis and their utility in advanced applications of transition metal oxides represent an exciting and rapidly expanding research area. Several techniques are being used to take control over the size to seize the potential applications of transition metaloxides[1]. In particular molybdenum oxide has attractive and unusual chemistry produced by the multiple valance states among the transition metal oxides[2-3]. Molybdenum oxide at nanoscale has shown high activity and being used in diverse applications such as cathodes in rechargeable batteries, field emission devices, solid lubricants, superconductors, thermoelectric materials, electrochromic devices and as a photocatalyst[4-8].

Molybdenum oxide has binary oxides, (MoO_2 and $MoO_{3)}$. Molybdenum trioxide has several polymorphs, such as the thermodynamically stable orthorhombic α-MoO_3, metastable monoclinic β-MoO_3 and hexagonal metastable h-MoO_3. The crystalline structure of orthorhombic α-MoO_3 unique layer structure made up of chains of octahedra that share corners. Two such chains are connected by sharing two edges of the octahedra to form a double chain. These double chains are then connected together in the third dimension (perpendicular to the plane of the double chain) by sharing corners to form a sheet-like structure. Thus for each octahedron, three oxygen atoms are shared by three octahedra of the same double chain, two are shared by two octahedra of adjacent double chains, and one is unshared. This unshared unit is commonly referred to as a Mo=O unit. Finally, these two dimensional sheets are stacked on top of each other with rather weak interaction van der Waals' forces between layers[9]. MoO_3 having wide band gap of 2.5 to 3.2 eV, an n-type semiconductor and a promising material for photocatalytic degradation of organic molecules both under UV and visible light. It has been used in different technical, industrial and in scientific application. It has been investigated over the past decades due to its distinctive

properties of electrochromism, thermochromism and photochromism, as smart materials, gas sensors, lubricants, electrochemical storage, catalysts and host materials for intercalation[10-13].

The formation of +4 and +6 oxidation states of molybdenum in molybdenum oxide with required phase and the novel characteristic properties differing from their bulk counterpart mainly depends on the method of synthesis. Considerable research effort has concentrated on synthesizing MoO_3 nanostructures with specific morphologies, sizes, crystal structures, and dopant using various synthesis techniques including sol−gel, combustion, hydrothermal synthesis, chemical vapour deposition and pulsed laser ablation[14-21].Among these methods, solution combustion route is promising as one can control the product formation by controlling the several parameters such as oxidizer to fuel ratio, volume of the precursor solution, reaction temperature, oxygen/air partial pressure, additional oxidizers, mixture of fuels and ignition temperature. This process is capable of producing larger-scale materials, faster, and lower-temperature syntheses.

Redox active metal oxide materials have become the centre of attraction for the supercapacitor studies[22]. The process of charge storage is a combination of two mechanisms in case of metal oxides [23]. These materials store energy through highly reversible surface redox reactions in addition to electric double layer capacitance; this is termed as pseudocapacitance [24,25]. Redox active metal oxides have gained considerable interest in the areas of electrochromics and batteries [26,27]. The electrochromic effect exhibited by these materials has made them very useful in the development of displays and smart windows [28,29].

In the present work, MoO_3 have been synthesised by solution combustion method starting with dissolving Mo metal powder in hydrogen peroxide and using sucrose as a fuel within few minutes. The particle size varies in the range of 2-10 nm. Electrochemical studies have not only been used to characterize, but also to examine the specific capacitance and

electrochromic properties of both the metal oxides that were synthesized. MoO_3 has shown an excellent photocatalytic activity for the degradation of Methylene blue under UV light.

The present combustion synthesis using molybdenum metal as precursor and sucrose as fuel has several advantages of short reaction time, use of low cost precursors and high exothermicity which last in few seconds leads to controlled particles growth producing floppy end product.

2. Experimental

2.1 Synthesis: Synthesis of MoO_3 has been carried out using two different sources of Mo. Syntheses routes 1 and 2 provide the preparation of molybdenum oxide using precursor solutions of Mo metal and ammonium heptamolybdate pentahydrate $(NH_4)_6Mo_7O_{24}.\ 5H_2O$ (AHM) respectively. All chemicals were purchased from Merck Ltd. and used without further purification.

Synthesis route 1: An aqueous solution of peroxopolymolybdic acid was prepared by dissolving 0.2 g of molybdenum metal powder by adding 3 mL of hydrogen peroxide (28%) in 100 mL beaker. About 0.37 g of sucrose was added into this solution as a fuel (Oxidizer:Fuel ratio=1:1). The mixture was heated on a hot plate at 150 ± 5 °C for 2-3 min to get homogeneous aqueous solution. The aqueous solution mixture was then placed into a muffle furnace maintained at 470±10 °C in air atmosphere. A vigorous flammable reaction with voluminous froth formation lead to the final products in one minutes and this powder is labelled as M1.

Synthesis route 2: In this section, a precursor solution was prepared by dissolving 0.5 g of AHM in 5 mL distilled water taken in 100 mL beaker. Upon warming, a clear light green solution was formed. To this, 1.71 g of DL-malic acid was transferred, and in succession, the greenish coloured solution mixture turned dark blue. This aqueous solution mixture was then placed into a muffle furnace maintained at 470±10 °C. After about 5 min, froth formation

followed by smouldering combustion was observed. The powder obtained by this route is labelled as M2.

2.2 Electrochemical procedures

Electrochemical measurements have been carried out using three electrode cell systems. Glassy carbon electrode (GCE), platinum electrode and saturated calomel electrode were used as working, counter and reference electrodes respectively. Uniform suspension of synthesized metal oxide in double distilled water with 5 mg mL^{-1} concentration was obtained by ultrasonicating the mixture for 20 min. 6 μL of this suspension was drop casted on to the GCE and left dried in the ambient air. Before that GCE was washed with 1, 0.3 and 0.05 micron alumina slurry and then with distilled water.

Indium tin oxide (ITO) coated clear and transparent glass electrode of 2 cm x 1 cm x 0.7 mm was washed with alcohol and deionized water. Water suspension of metal oxide was drop casted onto the glass electrode and dried under ambient conditions.

Cyclic voltammetry (CV) Procedure: 10 mL of 0.5M H_2SO_4 was taken in the electrochemical cell as an electrolyte and nitrogen gas was purged for 15 minutes to remove the dissolved oxygen. Using three electrode system voltammograms were recorded.

2.3 Photocatalytic MB degradation

The photocatalytic activity of as synthesized molybdenum oxide (M1) was evaluated by measuring the photocatalytic degradation of Methylene blue (MB) in water under the illumination of UV-light. A 120 W high pressure mercury lamp with wavelength of 253 nm was used as UV-irradiation source. In a typical degradation experiment, 250 mL of MB solution with a concentration of 75 mgL^{-1} and 100 mg prepared molybdenum oxide (M1) were added into a 500 mL Pyrex dish. The pH of this solution mixture was ~7. At a regular

time intervals of 5 min, 3 mL of aliquots were sampled and centrifuged to remove the oxide particles. The degradation of the organic dye was monitored by measuring the absorbance of the aliquot solution using the UV-visible spectrophotometer with de-ionized water as reference. The characteristic absorption of MB at 664 nm was chosen as the parameter to be monitored for the photocatalytic degradation process.

3. Characterization

The powder XRD pattern was recorded on a PANalytical X'pert PRO X-ray diffractometer with graphite monochromatized Cu Kα radiation source (λ = 1.541 Å). Morphologies and particle size of combustion derived powders were examined using JEOL-JSM–6490 LV scanning electron microscopy (SEM) and high resolution transmission electron microscopy (HRTEM) by JEOL JEM 2100 operating at 200 kV. IR spectra were recorded using a Bruker Alpha-T FTIR spectrometer (Diamond crystal ATR mode, resolution 4 cm^{-1}, 400–4000 cm^{-1}). Thermogravimetric and differential thermal analyses were performed from room temperature to 1000 ^{0}C with heating rate of 10 ^{0}C/min using SDT Q600 V20.9 Build 20 apparatus. Cyclic voltammetry experiments were performed using CH Instruments electrochemical work station (Model CHI 619B, CH Instruments, TX, USA) in a standard three electrode cell.

4. Results and discussion

The powder X-ray diffraction patterns of as prepared MoO_3 powders (M1 and M2) are shown in Figure 1. All the Braggs' reflections of M1 and M2 powders could be indexed to an orthorhombic phase of MoO_3. The sharp diffraction peaks of MoO_3 at *(020), (110), (040), (021)* and *(060)* indicates a highly crystalline orthorhombic structure (α-Phase). The intensity of the diffraction peak of *(021)* planes is very strong as shown in Figure 1a, indicating a crystal orientation along *(001)*. In Figure 1b intensified peaks of *(020)* planes of the powder

XRD pattern suggests that the obtained material has an anisotropic orientation with the *(010)* face[30]. The broadening of PXRD pattern of M1 powder indicates the smaller crystallite sizes. The crystallite sizes calculated using the Williamson-hall plot obtained by profile fitting of XRD spectra of MoO_3 powders of M1 and M2 respectively found to be 18 nm and 50 nm.

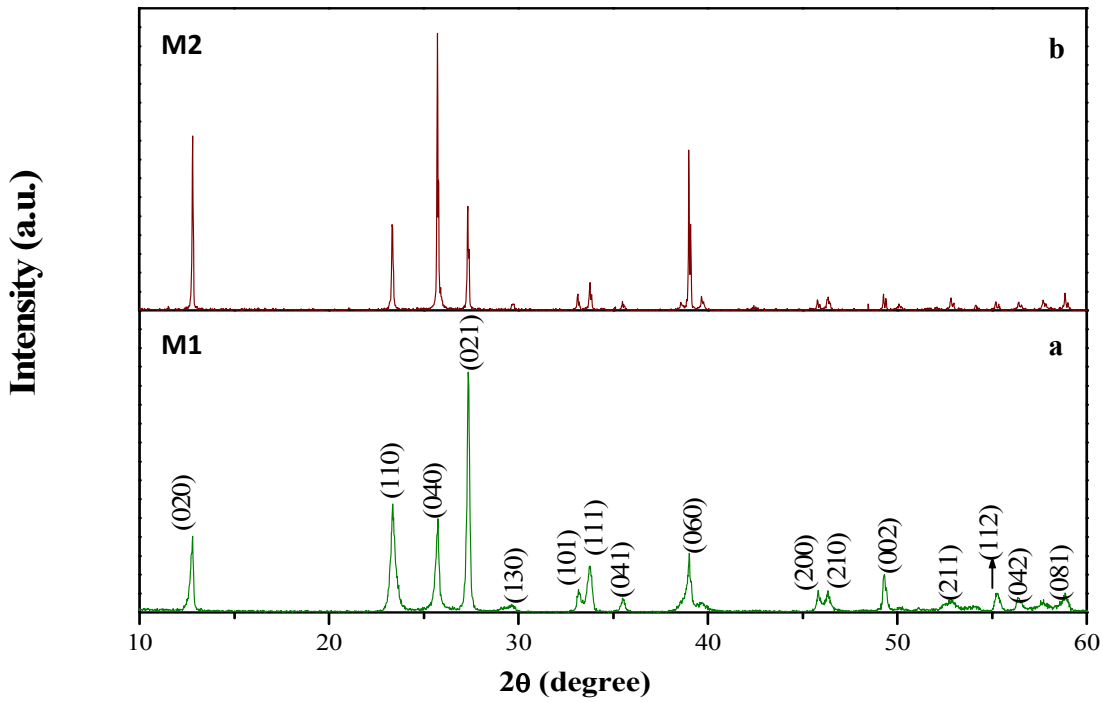

Figure 1. PXRD patterns of MoO_3 powders: (a) M1 powder and (b) M2 powder

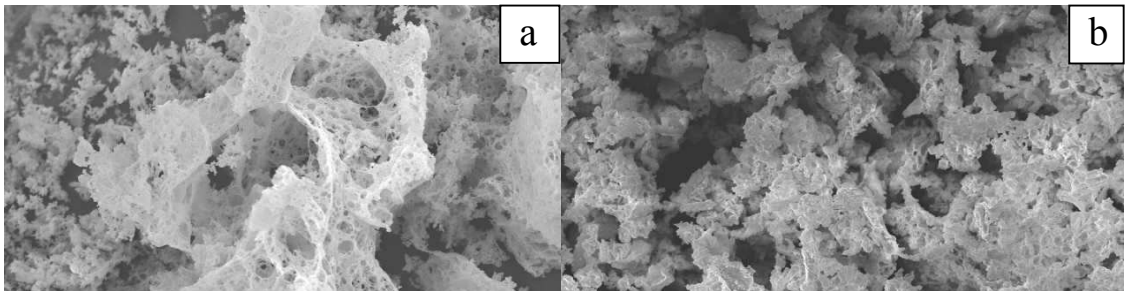

Figure 2. SEM images of MoO_3 powders: (a) M1 powder and (b) M2 powder

Morphological evolutions of as synthesized MoO_3 powders (M1 and M2) have been studied using SEM micrographs. Figure 2a is the SEM image of the M1 exhibiting macroporosity with fine grains. BET surface area is found to be ~4.97 m^2g^{-1}. Figure 2b is the SEM image of M2, despite showing porous it is quite agglomerated.

Figure 3 shows the TEM images, SAED pattern and size distribution histogram of MoO_3 (M1) powder. From TEM images (a and b), it is observed that the particles are well distributed and less agglomerated. The abundance of particles with different size is also shown in Figure 3d with a size distribution histogram. It is evidenced that narrow particle size distribution with highest frequency in the range of 6±2 nm. The histogram was obtained by analyzing several frames of similar bright field images using IMAGE J software. The selected area electron diffraction (SAED) pattern (Figure 3c) shows polycrystalline nature of MoO_3 (M1) powder. TEM image of M2 powder is shown in SI (Figure S5) and it is found that the particles are in the range 50 to 100 nm.

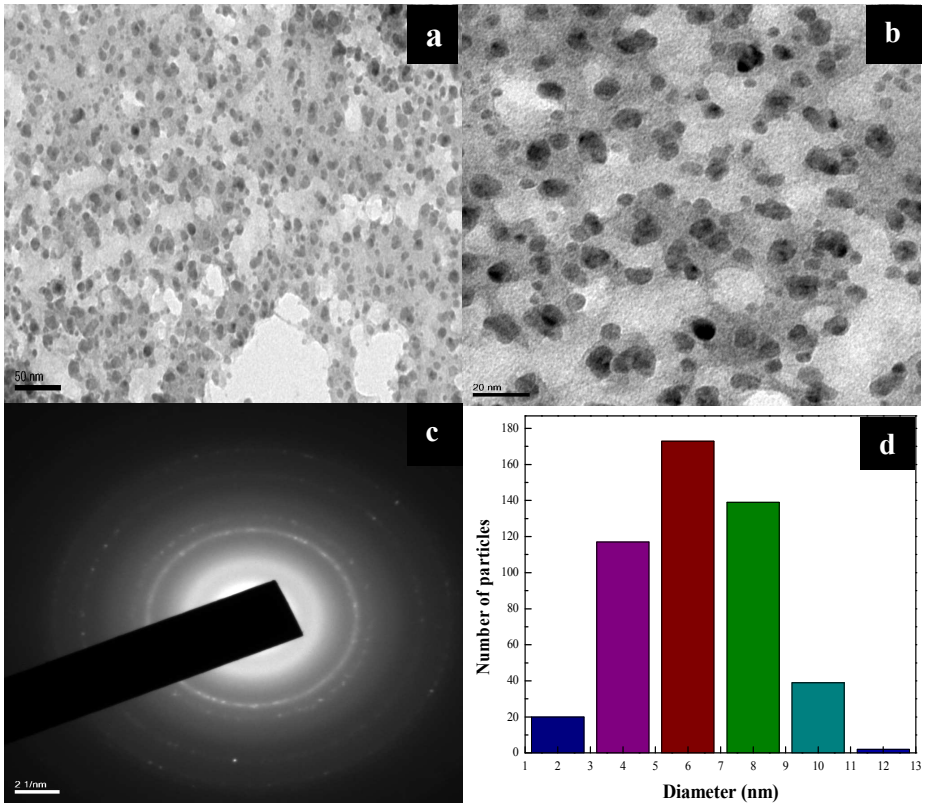

Figure 3. TEM images (a and b), SAED pattern (c) and size distribution histogram (d) of MoO_3 (M1) powder

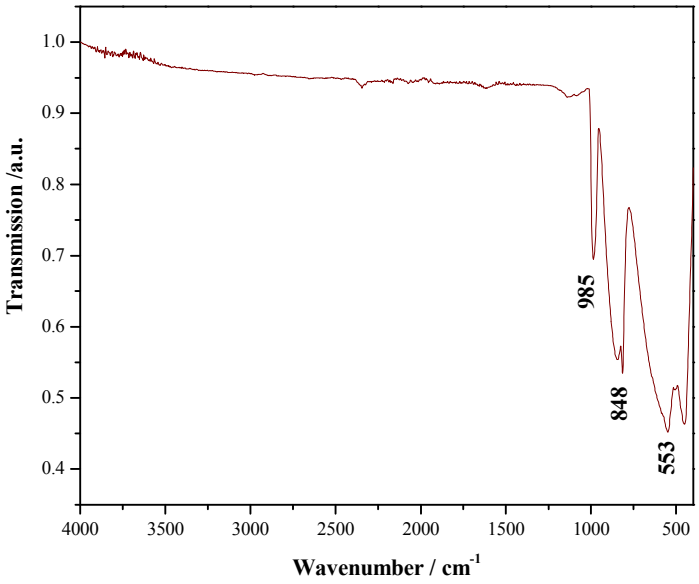

Figure 4. IR spectrum of MoO_3 (M1) powder

FT-IR was performed to investigate chemical bonding states between molybdenum and oxygen atoms in MoO_3. Figure 4 shows the IR spectrum of MoO_3 (M1) measured in 4000-400 cm^{-1} region. It can be seen that the as-prepared MoO_3 shows three peaks at 553, 848 and 985 cm^{-1}. The peak at 985 cm^{-1} is due to the terminal Mo=O bond, which is an indicator of the layered orthorhombic MoO_3 phase. The peak at 848 cm^{-1} is attributed to the Mo-O-Mo vibrations of Mo^{6+} ions and the broad band at 553 cm^{-1} to the bending vibration of oxygen atom linked to three metal atoms[31].

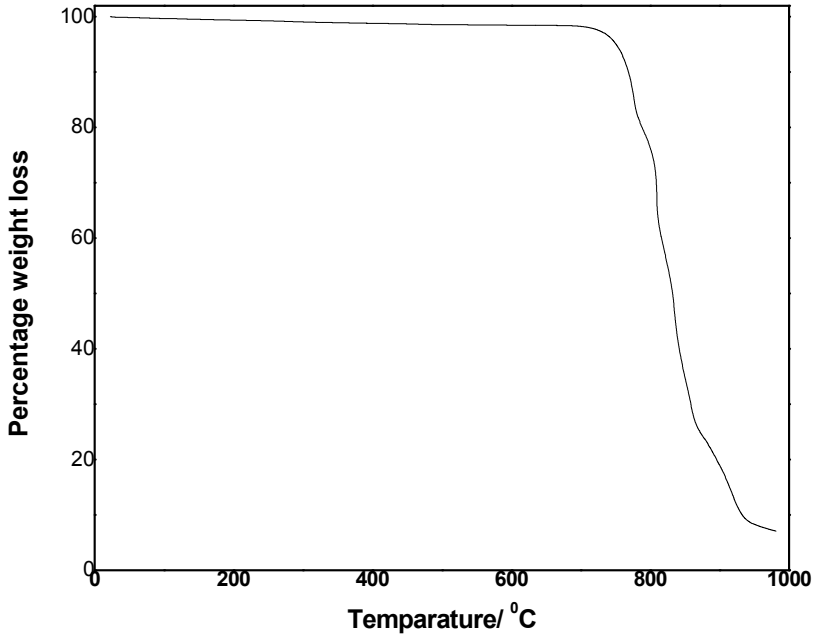

Figure 5. TGA of as synthesised MoO_3 (M1) powder

TGA was performed to verify the presence of carbon content in the as synthesised MoO_3 (M1) powder. Figure 5 shows that there is very less weight loss of ~1.54% till 700 °C which is negligible and could be accounted for the adsorbed water.

4.1 Electrochemical studies

MoO_3 (M1) powder drop casted GCE as working electrode and by following the above described CV procedure 25 continues cyclic voltammograms were recorded in a potential window from -0.8 to +0.6 V with a scan rate of 30 mVs^{-1}. Three sets of well resolved and reversible redox couples were observed at -0.032, -0.409 and -0.55 V as shown in Figure 6. Similar studies have been extended to M2 and commercial MoO_3 for the comparison purpose with the same experimental conditions are shown in SI Figure S1 and S2.

In reported literature also one can find the three sets of redox peaks. But the difference in the peak current and potential corresponding to major redox peak will be due to different experimental conditions and different electrodes employed[32]. In the above described potential window during the cathodic half cycle hydrogen ions insertion takes place into the M1 film that result in the formation of hydrogen molybdenum oxide bronzes [Equation 1]. During the reverse cycle deinsertion of hydrogen ions takes place to form the low-valent molybdenum oxide [Equation 2][33]. Though this process is reversible, there is a decrease in the peak currents can be observed due to the trapping of certain percentage of inserted hydrogen ion[34].

$$MoO_3 + xH^+ + xe^- \rightarrow MoO_{3-x}(OH)_x \quad (0<x<1.6) \qquad (1)$$

$$MoO_3 + 2ye^- + 2yH^+ \rightarrow MoO_{3-2y} + yH_2O (0<y<1) \qquad (2)$$

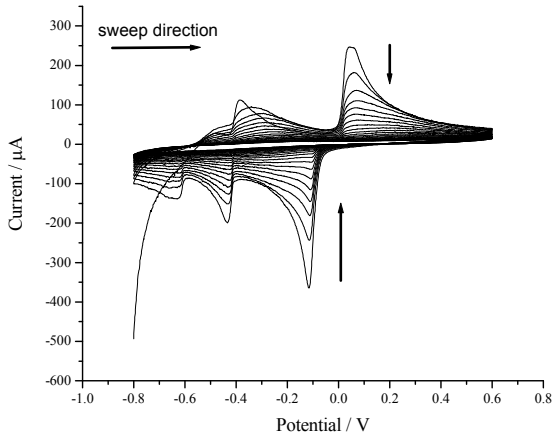

Figure 6. Continues cyclic voltammograms (25 cycles) of MoO_3 (M1) powder drop casted GCE in 0.5 M H_2SO_4 with a scan rate 30 mVs^{-1}.

The specific capacitance of the M1 drop casted GCE has been determined by recording the CV in potential window 0.2 to 1.2 V with 40 mVs^{-1} scan rate by following the above described procedure. Similarly CV has been recorded for M2 and commercially obtained MoO_3 for the comparison purpose and provided in the SI Figure S1 and S2. Cyclic voltammograms obtained for synthesized MoO_3 systems was little different from the rectangular shape and it consists of one redox peak (Figure. 7). Capacitance and specific capacitance (C_{sp}) were calculated using the equations (3) and (4) [17]. C_{sp} of the M1, M2 and commercially procured MoO_3 systems were found to be 108.88, 77.09 & 41.04 Fg^{-1} respectively.

$$\mathbf{C_{sp} = 2C_{dl}/S}$$ ……..Equation (3)

Where, C_{sp} – specific capacitance

C_{dl} – double layer capacitance

S – quantity of the material used for the study (in this particular case, quantity of material drop casted onto the electrode)

Double layer capacitance was calculated using the formula:

$$C_{dl}\,(dE/dt) = (I_a - I_c) / 2 \text{.....Equation (4)}$$

Where, C_{dl} – double layer capacitance

dE/dt – rate of change of potential (scan rate) at which voltammogram recorded

I_a – anodic current

I_c – cathodic current

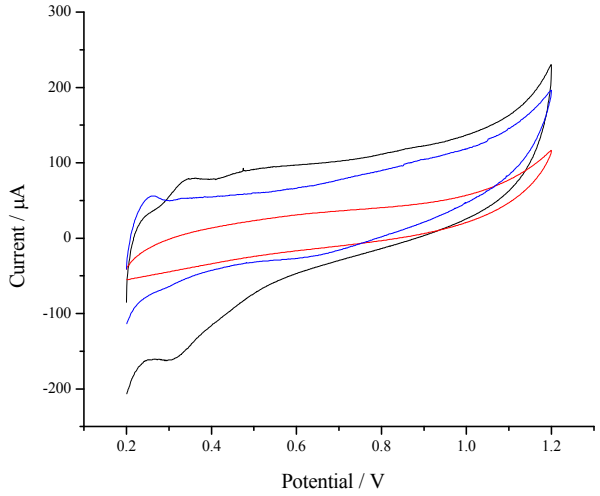

Figure 7. Overlaid cyclic voltammograms of M1 (black line), M2 (blue line) and commercially obtained MoO_3 (red line) drop casted GCE in 0.5 M H_2SO_4 with 40 mVs^{-1} scan rate

Redox reactions explained in equations 1 and 2 reins the electrochromic property of MoO_3. As explained in equation 1, cathodic polarization at -2.0 V of M1 casted ITO coated glass causes the intercalation of H^+ ions that in turn converts the white film to green colored one. The intensity of the green color can be increased by polarizing the film at higher cathodic over potential such as -3.0 V. The reverse of the above i.e. anodic polarization causes the deintercalation of inserted H^+ ions that leads to the bleaching of colored film. Further anodic polarization at +3.0 V causes the complete bleaching of green color as shown in Fig. 8a. The

corresponding transmittance spectra were recorded for the different polarizations applied. Spectra agree well with the optical photos and above explanation. With the increase in cathodic polarization potential green color gets intensify hence the decrease in transmittance can be observed. Inversely with increase in anodic polarization potential bleaching of the color of the film will be more hence the M1 film becomes more transparent (Figure 8b). Whereas M2 and commercial MoO_3 also forms the molybdenum bronze like M1 due to the intercalation of H^+ ions on applying the potentials such as -2.0 and -3.0 V shown in SI Figure S3 and S4 respectively. But the colour intensity of M1 > M2 > commercial MoO_3 at the same applied potentials. This indicates the greater percentage of insertion of H^+ into MoO_3 in case of M1. Similarly less bleaching of colour in case of M2 and commercial MoO_3 has been observed compared to M1. This can be explained due to incomplete deintercalation of inserted H^+ ions due to less porosity.

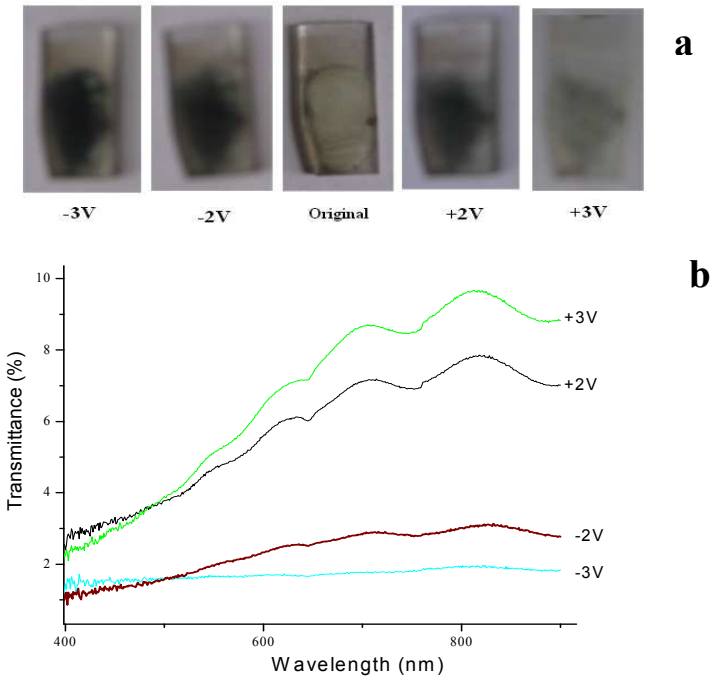

Figure 8. (a) Optical photos of MoO_3 (M1) casted ITO coated glass after applying the different polarization potentials in a chronological order -3, -2, 0, +2, +3 V for 120 s. (b) corresponding UV-Vis spectra of the M1 coated ITO glass.

4.2. Photocatalytic activity

The photocatalytic degradation of MB was used as a test reaction to investigate the photocatalytic performance of MoO_3 (M1) nanoparticles. There are several reports of photocatalytic degradation of MB[35] and here we are investigating under UV irradiation. The degradation was monitored by UV-vis absorption spectroscopy by using characteristic light absorption of MB at 664 nm at prefixed time interval.

Initially with constant concentration of MB dye, the influence of amount of photocatalyst was investigated in the range of 50 to 250 mg. Around 100% degradation was observed with the dye concentration of about 75 mgL^{-1} at 100 mg of catalyst.

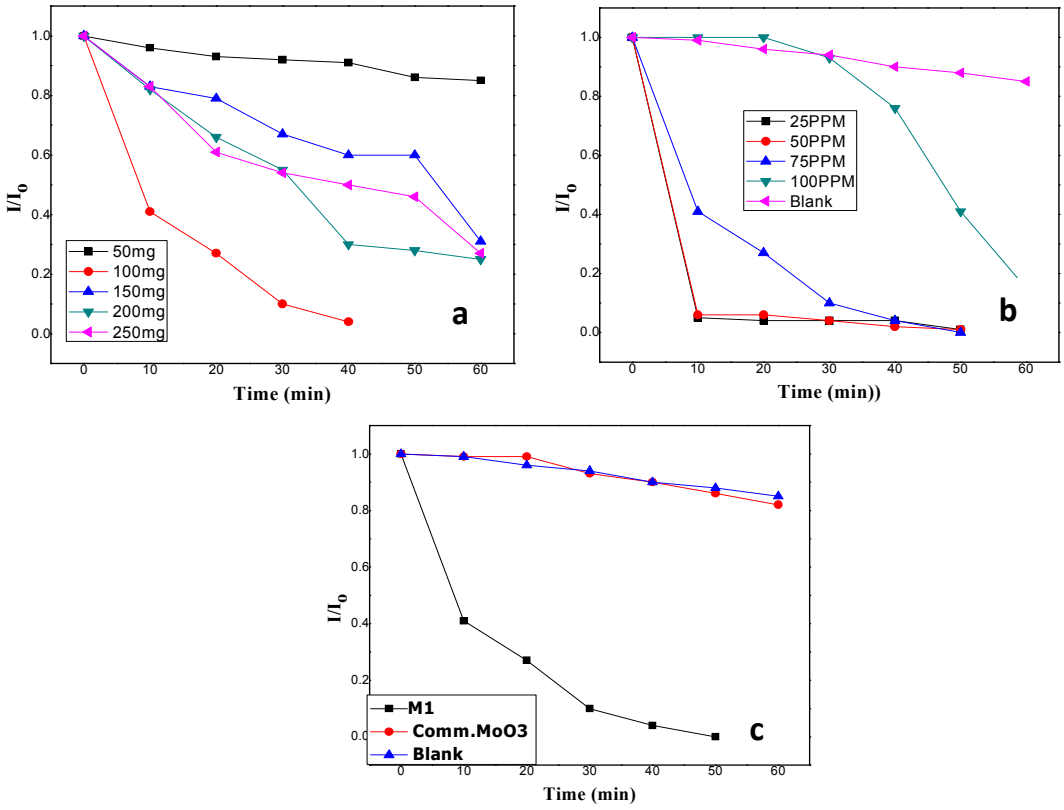

Figure 9. .Photocatalytic degradation of MB: (a) at constant concentration of 75 mg L^{-1} over a range of catalyst load, (b) at constant catalyst dosage of 100 mg over a range of concentration and (c) comparison of MoO_3 (M1) with commercial MoO_3

Figure 9a shows I/I_o versus irradiation time, where I and I_o are the intensities of the absorbance peak at 664 nm at the reaction time and the initial time. With lower catalyst dosage the degradation was very poor as we can see with the 50 mg of catalyst only ~ 10% degradations. Even with increase in the catalyst dosage more than 100 mg shows lower degradation. This might be due to the scattering of UV light by the excess of photocatalyst which reduces the generation of charge carriers. The other reason could be the turbidity arised due to the high catalyst dosage which in turn due to the aggregation of the catalyst particles leads to a decrease in the penetration of light.

As the catalyst dosage has been optimised, the effect of concentration was investigated. Figure, 9b shows as the dye concentration increase to 100 mgL^{-1} there was large decrease in the degradation rate. Hence the optimum catalyst doses of 100 mg MoO_3 can degrade 75 mgL^{-1} of MB in 60 min. But the commercial MoO_3 shows nearly 18% of degradation even after 60 min.

4. Conclusion

In summary, we have established combustion reaction that could produce orthorhombic MoO_3 nanoparticles. As made MoO_3 powders (M1 and M2) exhibited electrochromic properties besides photocatalytic activity in the degradation of methylene blue. Another interesting point of MoO_3 (M1) powder is with fine particles size in the range of 2-10 nm having surface area of ~4.97 m^2g^{-1}. Hence, this high photocatalytic activity could be correlated with the narrow size distribution of the synthesised MoO_3 (M1) powders.

Acknowledgements

One of the authors, G.T. Chandrappa thanks Department of Science and Technology (DST), Government of India, New Delhi for financial support to carry out the present research work.

References

1. B. Nagappa, G. T. Chandrappa, J. Livage, *Pramana,* **2005**, *65,* 917.
2. N. A. Chernova, M. Roppolo, A. C. Dillon, M. S. Whittingham, *J. Mater. Chem.* **2009**, *19,* 2526.
3. D. O. Scanlon, G. W. Watson, D. J. Payne, G. R. Atkinson, R. G. Egdell, D. S. L. Law, *J. Phys. Chem. C,*.**2010**, 114, 4636.
4. M. Labanowska, *ChemPhysChem*., **2001**, 2(12), 712.
5. A. M. Taurino, A. Forleo, L. Francioso, P. Siciliano, M. Stalder, R. Nesper, *Appl. Phys. Lett.,* **2006**, 88, 152111.
6. J. Zhou, N. –S. Xu, S. –Z. Deng, J. Chen, J. –C. She, Z. –L. Wang, *Adv. Mater.,* **2003**, 15, 1835.
7. T. Itoh, I. Matsubara, W. Shin, N. Izu, M. Nishibori, *Sensor Actuat B-Chem.,***2008**, *128,* 512.
8. J. N. Yao, K. Hashimoto, A. Fujishima, *Nature.* **1992**, 355, 624.
9. T. Brezesinski, J, Wang, S. H. Tolbert, B. Dunn, *Nature materials.,* **2010**, 9, 146.
10. B. Guo, X. Fang, B. Li, Y. Shi, C. Ouyang, Y. Hu, Z. Wang, G. D. Stucky, L. Chen, *Chem. Mater.,* **2012**, 24, 457.
11. K. Sakaushi, J. Thomas, S. Kaskel, J. Eckert, *Chem.Mater,* **2013**, 25, 2557.
12. K. Hosono, I. Matsubara, N. Murayama, S. Woosuck, N. Izu, *Chem. Mater*. **2005**, 17(2), 349.
13. L. Q. Mai , B. Hu, W. Chen, Y. Y. Qi, C. S. Lao, R. S. Yang, Y. Dai, Z. L. Wang. *Adv. Mater.,* **2007**, *19,* 3712.
14. C. V. Krishnan , J. Chen , C. Burger, B. Chu, *J. Phys. Chem. B*, **2006**, 110, 20182.
15. G. Zhao, N. Zhang, K. Sun. *J. Mater. Chem. A***. 2013**, 1, 221.

16. I, Shakir, M. Shahid, D. J. Kang. Chem. Commun., **2010**, 46, 4324.

17. M. B. Sreedhara, H. S. S. R. Matte, A. Govindaraj, C. N. R. Rao. *Chem. Asian J.* **2013**, 8, 2430.

18. D. Parviz, M. Kazemeini, A. M. Rashidi, K. JafariJozani, *J Nanopart Res.,* **2009**, 12, 1509.

19. A. Lagashetty, V. Havanoor, S. Basavaraja, A. Venkataraman, *Mater. Res. Bull.,* **2005**, 28, 477.

20. G. P. Nagabhushana, G. Nagaraju, G. T. Chandrappa, *J. Mater. Chem. A*., **2013**, *1,* 388.

21. G. P. Nagabhushana, G. T. Chandrappa, *J. Mater. Chem. A*., **2013**, *1,* 11539.

22. Z. Lei, X. Yang, J. Dong, X. Yi, *J. Mater. Chem.,* **2010**, 20. 7135.

23. X. Mao-Wen, J. Wei, B. Shu-Juan, S. Zhi, D. Bin, Electrochimica Acta, **2010**, 55, 5117.

24. M. Nakayama, A. Tanaka, Y. Sato, T. Tonosaki and K. Ogura, *Langmuir*, **2005**, 21, 5907.

25. T. Y. Wei, C. H. Chen, H. C. Chien, S. Y. Lu, C. C. Hu, *Adv. Mater*, **2010**, 22, 1347.

26. C. G. Granquist, Handbook of Inorganic Electrochromic Materials, 1st ed., Elsevier, Amsterdam., 1995.

27. M. Winter, J. O. Beshard, M. E. Spahr, P. Novak, *Adv. Mater*., **1998**, 10, 725.

28. U. Bach, D. Corr, D. Lupo, F. Pichot, M. Ryan, *Adv. Mater*., **2002**, 14, 845.

29. C. Sella, M. Maaza, O. Nemraouti, J. Lafait, N. Renard, Y. Sampeur, Surface and Coatings Technology, **1998**, 63, 199.

30. S. Guimond, D. Göbke, J. M. Sturm, Y. Romanyshyn, H. Kuhlenbeck, M. Cavalleri, H, –J, Freund, *J. Phys. Chem. C.*, **2013**, *117,* 8746.

31. H. C. Zeng, *Inorg. Chem.,* **1998**, 37, 1967.

32. V. S. Saji, C. W. Lee, ChemSusChem., **2012**, 5, 1146.

33. W. Baoxing, D. Shaojun, *J Electroanal Chem.*, **1994**, 379, 207.

34. J. T. Hupp, X. Dang, *Langmuir,* **2003**, 19, 4316.

35. A. Chithambararaj, N. S. Sanjini, A. Chandra Bose and S.Velmathi, *Catal. Sci. Technol.*, **2013**, 3, 1405.